Using the nonhydrodynamic mode to study the onset of hydrodynamic behavior in ultraperipheral symmetric nuclear collisions

Nikhil Hatwar [*] and M. Mishra[†]

Department of Physics, Birla Institute of Technology and Science, Pilani, Rajasthan 333031, India

With the attempts of extending the hydrodynamic framework of heavy-ion collision to proton-proton and other small and low-energy systems, we are confronted with the question of how small the system can get and still be safely modeled as a fluid. One of the transport coefficients required in the second-order relativistic viscous hydrodynamics is the shear relaxation time, inclusion of which solves the causality violation problem in the Navier-Stokes equation. In phenomenological studies this coefficient has been taken as a constant and much attention has gone into finding and fixing the shear viscosity to entropy density ratio, η/s. This transport coefficient also happens to control the nonhydrodynamic mode of the out-of-equilibrium hydrodynamics theory. It has been predicted that for decreasing system size, observables become sensitive to variation in shear relaxation time as a result of increasing dominance of the nonhydrodynamic mode, which could potentially indicate the breakdown of hydrodynamics. In this study, we try to test this prediction in peripheral Pb-Pb collisions at 2.76 TeV and Au-Au collisions at 200 GeV, with IPGlasma initial condition and $(2+1)$-dimensional viscous hydrodynamics. We find that elliptic flow does show adequate sensitivity to variation in relaxation time for decreasing system size. The multiplicity rapidity density limit for applicability of hydrodynamics is found to be around $dN/dy \approx 10$, with the possibility of refinement in this value given a way to improve the centrality resolution in experimental data for referencing in peripheral collisions.

I. INTRODUCTION

The fact that baryons have internal structure directly leads to the notion that a bulk medium of subnucleonic degrees of freedom should exist [1,2]. An energy density of about 0.7 GeV/fm^3 is required to free up quarks from the nucleons [3,4]. We now have convincing signs from experiments at the BNL Relativistic Heavy Ion Collider (RHIC) and the CERN Large Hadron Collider that indicate a deconfined state of quarks and gluons called quark-gluon plasma (QGP) is formed for a sufficient distinguishable duration. Low-order hydrodynamic constitutive relations apparently explain the experimental observables of such a dynamic system quite well, even though there is a sizable pressure anisotropy. This applicability of low-order hydrodynamics has been referred to as *hydrodynamization*,[1] to distinguish it from local thermalization [5,6]. Experimental confirmation of strangeness enhancement [7], elliptic flow [8], and jet quenching [9,10] as the early indicators was subsequently followed by confirmation of other signatures like quarkonia suppression. Efforts now are directed towards quantitatively fixing the boundaries of various regions of the quantum chromodynamics (QCD) phase diagram [11] and deducing the properties of QGP [12].

There are challenges involved in analytically solving nonperturbative QCD, making the proof of deconfinement intractable [13]. Hence, the progress in modeling a medium of quarks and gluons from first principles has been limited. Lattice QCD, even though computationally intensive, has been of help in understanding deconfinement and other low density phenomena where the numerical sign problem does not affect the calculations [14,15]. For now, phenomenological models aided by lattice QCD seem to be the right approach to modeling such a complex system. The use of hydrodynamics in modeling the transient QGP stage has been quite surprising [16]. However, hydrodynamics as an effective theory for heavy-ion collisions has evolved tremendously, especially in the last two decades. For an in-depth review of the hydrodynamics in heavy-ion collisions, please lookup Refs. [17–23]. Apart from the traditional conversation equation approach, hydrodynamics can also be derived as a microscopic theory in the limit, e.g., starting from kinetic theory or any quantum field theory (QFT) like QCD provided its dynamics show quasiuniversality at a large timescale [21]. This microscopic theory approach also helps in fixing the transport coefficients of the theory [18].

---

[*]nikhil.hatwar@gmail.com

[†]madhukar@pilani.bits-pilani.ac.in

[1]In this study, we refer to the applicability of low-order hydrodynamics as "hydrodynamization," in accordance with its definition in Ref. [5].

The energy-momentum tensor for such a theory in a nonequilibrium state is decomposed as

$$T^{\mu\nu} = \langle T^{\hat{\mu}\nu} \rangle_{\text{eq}} + \delta\langle T^{\hat{\mu}\nu} \rangle, \quad (1)$$

where the first and second terms represent the equilibrium state of $T^{\mu\nu}$ and the deviation from the equilibrium, respectively. Under linear response theory, the second term can be expanded as

$$\delta\langle T^{\hat{\mu}\nu} \rangle(x) = -\frac{1}{2} \int d^4 y\, G_R^{\mu\nu,\alpha\beta}(x^0 - y^0, \mathbf{x} - \mathbf{y}) \delta g_{\alpha\beta}(y), \quad (2)$$

where $G_R^{\mu\nu,\alpha\beta}(x^0 - y^0, \mathbf{x} - \mathbf{y})$ is the retarded two-point correlator of $T^{\mu\nu}$, and $\delta g_{\alpha\beta}(y)$ is a small perturbing term added to the flat space-time metric. This correlator when expressed in the Fourier space $[G_R^{\mu\nu,\alpha\beta}(\omega, \mathbf{k})]$, where ω is the angular frequency and $\mathbf{k}$ is the momentum, has singularities. The solution of the $\delta\langle T^{\hat{\mu}\nu} \rangle(x)$ integral at late times has a contribution in terms of a complex singular frequency in the ω plane:

$$\omega_{\text{sing}} = \omega_{\text{h}} + i\omega_{\text{nh}}, \quad (3)$$

where ω_{h} is the real part of the frequency at singularity corresponding to excitation of equilibrium plasma, also called the *hydrodynamic mode frequency*. ω_{nh} is termed as the transient mode or the *nonhydrodynamic mode frequency* and is associated with the dissipative effects. The transient mode is responsible for disruption of the hydrodynamization process and is controlled with the *relaxation time* parameter, which sets the duration for which viscous effects remain active. These are called the *quasinormal modes* of out-of-equilibrium hydrodynamics, analogous to the *normal modes* of oscillatory systems in classical mechanics.

Right after the collision of heavy ions, we have a nonequilibrium system of partons for up to 1 fm/c. The fact that applying low-order hydrodynamics does not require local thermalization or even pressure isotropy to show agreement with the measurements [23] had been puzzling, until we discovered that this evolution leads to an attractor [24–27]. This attractor guides the system evolution to a late-time universal trajectory even if initiated with a varied set of starting conditions [28].

The framework of hydrodynamics with initial conditions, followed by a hadron afterburner, has been quite successfully used to explain experimental data obtained from a wide range of systems [29,30]. From most-central to ultraperipheral collisions, the system size decreases monotonically. For a constant collisional energy, there should be a system size below which the QGP droplet will cease to *hydrodynamize* [31]. Kurkela *et al.* [32,33] has performed a flow analysis with kinetic theory leading to hydrodynamization, through a dimensionless physical quantity called opacity($\hat{\gamma}$)—a measure of transverse system size in units of the mean free path. As the opacity varies from 0 to 5, the system goes through three stages in this order: (a) a non-QGP (particlelike) stage, (b) an intermediate transition stage, and (c) a QGP (hydrolike) stage. Heinz and Moreland [34] have emphasized considering the multiplicity rapidity density of charged particles—dN/dy along with Hanbury Brown and Twiss (HBT) radii to quantify the smallest QGP size. According to Romatschke [23], the

large p_T regime of flow is due to the nonhydrodynamic mode and this mode can be studied through the relaxation time approach. He suggested that a large deviation of the elliptic flow (v_2) for a variation in shear relaxation time for lowering multiplicity could potentially indicate the breakdown of low-order hydrodynamics. The last two of the above studies came to the conclusion that this limit should be around or below $dN_{\text{ch}}/dy \approx 2$.

The role of relaxation time has been previously analyzed for different settings in hydrodynamics studies [16,35–39], including spatial and momentum eccentricity, entropy, and elliptic flow for varying relaxation times. However, the primary focus of these studies was to find the range of τ_π and other second-order transport coefficients for which the observables were insensitive, which in turn meant that the magnitudes of the second-order gradient terms are smaller in comparison to those of first-order gradient. In the present work, we check the sensitivity of observables to shear relaxation time in ultraperipheral collision systems to test the breakdown of low-order hydrodynamics. In Sec. II we discuss the framework of the model used. In Sec. II A, we state the initial condition and input parameters involved in the model. Section II B describes the observables obtained along with the experimental results in order to fix the centrality-related parameters. In Sec. III, we present results of elliptic flow as a function of the transverse momentum and the multiplicity rapidity density. And in Sec. IV, inferences are drawn based on results obtained along with the possible improvement to this work.

II. FORMALISM

Hydrodynamics is the collective dynamical evolution of a suitably sized bulk medium adhering to the system's symmetries. For the relativistic case, the conservation laws take the form $\partial_\mu T^{\mu\nu} = 0$ for the energy-momentum tensor and $\partial_\mu N^\mu = 0$ for the conserved charge. The local values of temperature $T(x)$, fluid velocity $u_\mu(x)$ and chemical potential $\mu(x)$ are chosen as hydrodynamic variables. For ultrarelativistic collisions, where a negligible amount of participating nucleons survive, the conservation equation for the baryon number ($\partial_\mu N^\mu = 0$) can be ignored. The energy-momentum tensor can be decomposed as [44]

$$T^{\mu\nu} = \epsilon u^\mu u^\nu + \Delta^{\mu\nu} P + (w^\mu u^\nu + w^\nu u^\mu) + \Pi^{\mu\nu}. \quad (4)$$

Here, ϵ (energy density) and P (pressure) are scalar coefficients, w^μ represents the transverse vector coefficient, $\Delta^{\mu\nu} \equiv g^{\mu\nu} + u^\mu u^\nu$ is the projector operator orthogonal to the fluid velocity (u^μ), and $g^{\mu\nu}$ is the space-time metric. The above expression without the $\Pi^{\mu\nu}$ term corresponds to 0th-order ideal hydrodynamics. The $\Pi^{\mu\nu}$ tensor is introduced to account for the dissipative effects and is further decomposed as

$$\Pi^{\mu\nu} = \pi^{\mu\nu} + \Delta^{\mu\nu} \Pi. \quad (5)$$

Π and $\pi^{\mu\nu}$ are the bulk and shear part of the viscous stress tensor. The forms of the shear stress tensor ($\pi^{\mu\nu}$) and the bulk pressure (Π) are set up in accordance with the covariant form of the second law of thermodynamics [17]. When we set the entropy four-current expression as $s^\mu = su^\mu$, where s is the

entropy density, we get

$$\pi^{\mu\nu} = \eta\sigma^{\mu\nu} \quad \text{and} \quad \Pi = \zeta\partial_\mu u^\mu, \qquad (6)$$

where η (shear viscosity) and ζ (bulk viscosity) are the transport coefficients, and $\sigma^{\mu\nu}$ (shear tensor) is a traceless, transverse, and symmetric tensor. This forms of $\pi^{\mu\nu}$ and Π lead to the first-order Navier-Stokes theory. When we introduce perturbations in energy density and fluid velocity, and evolve them, the diffusion speed obtained from the dispersion relation has a form that can increase arbitrarily. This theoretical formulation cannot be considered as a satisfactory one if it violates causality. It turns out that if the term $(-\tau_\pi u^\alpha \partial_\alpha \pi^{\mu\nu})$ is added in the expression of $\pi^{\mu\nu}$ above, the resulting diffusion speed stays below the speed of light. The coefficient of this newly added term, τ_π, is called the *relaxation time*. But this is still a makeshift way to restore causality in the system. A good second-order viscous hydrodynamics theory at the very least should reduce to the Navier-Stokes equation in the limit of long wavelengths and must show causal signal propagation.

Müller [45] and Israel and Stewart [46,47] (MIS) suggested modification of the entropy four-current expression used above to include the following term with a viscous stress tensor:

$$s^\mu = su^\mu - \frac{\beta_0}{2T}u^\mu\Pi^2 - \frac{\beta_2}{2T}u^\mu\pi_{\alpha\beta}\pi^{\alpha\beta} + O(\Pi^3), \quad (7)$$

where β_0 and β_2 are scalar coefficients. When we use this entropy four-current in the covariant second law of thermodynamics, the dissipative terms of the energy-momentum tensor take the following forms [17]:

$$\pi_{\alpha\beta} = \eta\left[\nabla_{\langle\alpha}u_{\beta\rangle} - \pi_{\alpha\beta}Tu^\mu\partial_\mu\left(\frac{\beta_2}{T}\right) - 2\beta_2 u^\mu\partial_\mu\pi_{\alpha\beta}\right.$$
$$\left. - \beta_2\pi_{\alpha\beta}\partial_\mu u^\mu\right], \qquad (8)$$

$$\Pi = \zeta\left[\nabla_\alpha u^\alpha - \frac{1}{2}\Pi\,T\,u^\mu\partial_\mu\left(\frac{\beta_0}{T}\right) - \beta_0 u^\mu\partial_\mu\Pi\right.$$
$$\left. - \frac{1}{2}\beta_0\Pi\partial_\mu u^\mu\right], \qquad (9)$$

where $\nabla^\mu = \Delta^{\alpha\mu}\partial_\alpha$ and $\nabla_{\langle\alpha}u_{\beta\rangle}$ is a symbol to represent traceless symmetrization of $\nabla_\alpha u^\beta$. A perturbative analysis with these newly obtained expressions leads to an inherently causal system. There are a few variants of this theory [48], depending on how many terms are kept in the $\pi^{\mu\nu}$ and Π expressions. The viscous hydrodynamics code used for this study is based on the MIS theory. The theory of Baier *et al.* [49] is a more comprehensive version of MIS hydrodynamics. A few third-order versions have also been worked up [50,51].

The second-order viscous hydrodynamics used for this study is a publicly available code (see Ref. [52]), ECHO-QGP [56,57], based on the MIS theory. It could be used in either (2 + 1)-dimensional (D) or (3 + 1)-D settings and has been utilized for bulk medium evolution in the study of quarkonia suppression [58]. The space-time evolution of all $T^{\mu\nu}$ components could be extracted at the output.

A tabular lattice QCD equation of state by the Wuppertal-Budapest Collaboration [59] has been utilized. In this

equation of state, the values for energy density (ϵ), speed of sound (c_s), and pressure (P) are available starting with a temperature of 100 MeV. In order to get values below this temperature we spline-interpolated temperature dependencies of quantities mentioned above with the corresponding values from a hadron resonance gas model [60]. Dissipative corrections to the energy-momentum tensor in ECHO-QGP are introduced in the same way as stated in Eq. (5). Here the evolution of the shear part of the viscous stress tensor is given by [56]

$$\pi^{\mu\nu} = -\eta\left(2\sigma^{\mu\nu} + \frac{4}{3}\frac{\tau_\pi}{\eta}d_\mu u^\mu\pi^{\mu\nu} + \frac{\tau_\pi}{\eta}\Delta^\mu_\alpha\Delta^\nu_\beta D\pi^{\alpha\beta}\right.$$
$$\left. + \frac{\lambda_0}{\eta}\tau_\pi\left(\pi^{\mu\lambda}\Omega^\nu_\lambda + \pi^{\nu\lambda}\Omega^\mu_\lambda\right)\right). \qquad (10)$$

Here, λ_0 is a scalar coefficient and Ω is a traceless, antisymmetric, transverse vorticity tensor. d_μ is the covariant derivative given by $d_\mu u^\nu = \partial_\mu u^\nu + \Gamma^\nu_{\beta\mu}u^\beta$, where $\Gamma^\nu_{\beta\mu}$ are the Christoffel symbols. $D = u^\mu d_\mu$ is the comoving time derivative. The evolution of the bulk part of the viscous stress tensor is given by

$$\Pi = -\zeta\left(d_\mu u^\mu + \frac{\tau_\Pi}{\zeta}u^\alpha d_\alpha\Pi + \frac{4}{3}\frac{\tau_\Pi}{\zeta}\Pi\,d_\mu u^\mu\right). \qquad (11)$$

The values of the transport coefficients τ_Π, λ_0, τ_π, η, and ζ are required for solving the above two equations, which are obtained from the microscopic theory approach to hydrodynamics. τ_Π is the bulk viscosity relaxation time, which represents how quickly the above second-order form of bulk
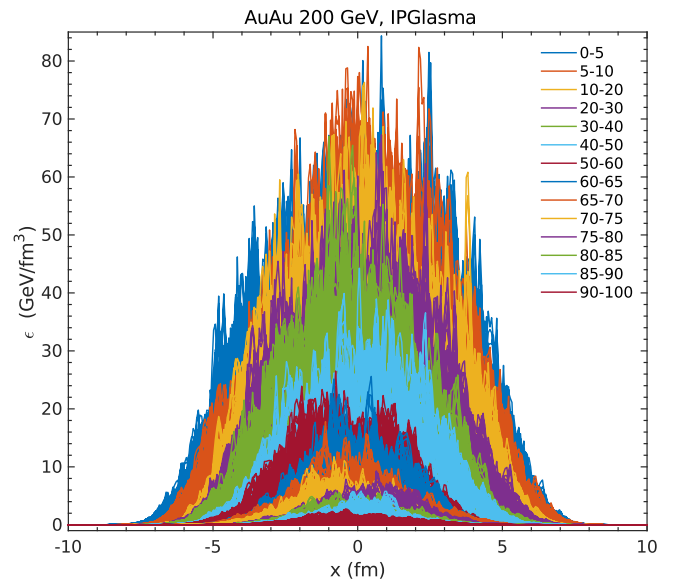

FIG. 1. Energy density distribution as a function of transverse coordinate at $\tau = 0.6$ fm produced at midrapidity for 14 centrality classes of Au-Au IPGlasma runs at 200 GeV. The distribution for each centrality class has been superimposed for 400 IPGlasma events with different nucleon positions to account for event-by-event fluctuations.
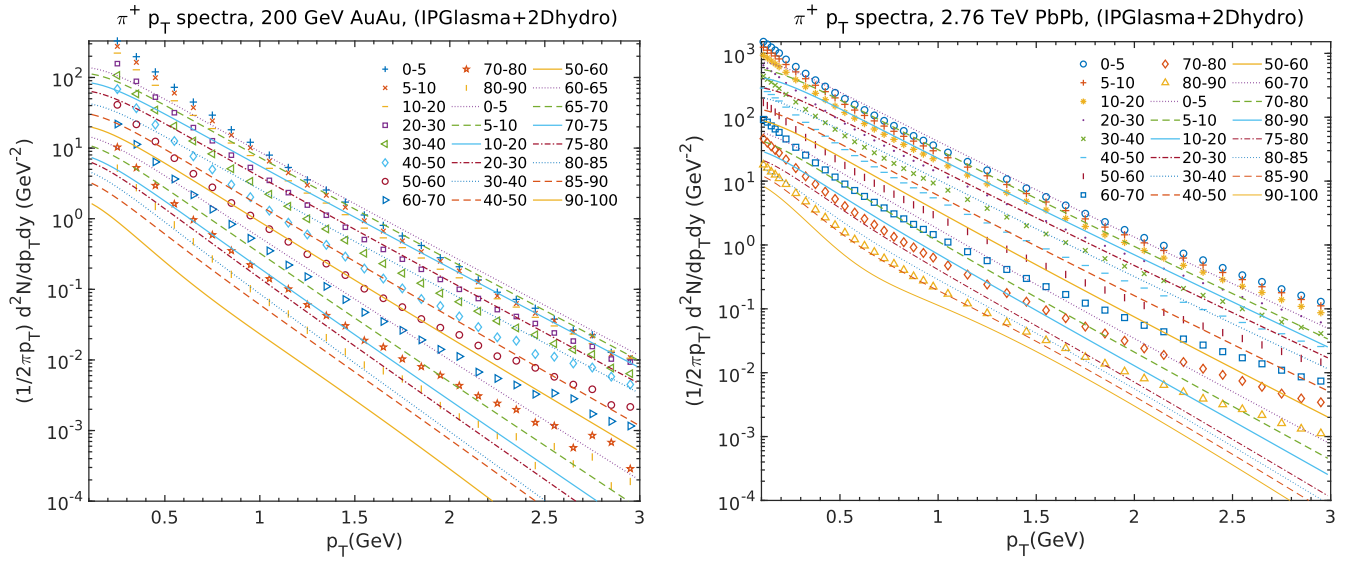
FIG. 2. Pion (π^+) p_T spectra generated (lines) for Au-Au at 200 GeV (left) and Pb-Pb at 2.76 TeV (right) for mentioned centrality classes compared with the corresponding PHENIX [40] and ALICE experimental results [41] (symbols).

pressure relaxes to its leading-order form in Eq. (6). The above two equations are derived under the metric signature choice of $(-1, +1, +1, +1)$.

A. Input parameters

The form of relaxation time has been worked out for hydrodynamics beginning from numerous microscopic theories, e.g., Boltzmann theory in the relativistic limit [47,61], weakly coupled QCD [62], and Anti–de Sitter/conformal field theory (AdS/CFT) [49,63,64]. In ECHO-QGP, the relaxation time is introduced as

$$\tau_\pi = \tau_{\text{coe}} \frac{\eta}{sT}. \quad (12)$$

The coefficient τ_{coe} here controls the magnitude of shear relaxation time in viscous hydrodynamics. In Sec. III, we see the consequence of varying this parameter on elliptic flow coefficients for Pb-Pb and Au-Au collisions. A transverse distribution of participating nucleons could serve as an initial condition for hydrodynamics. ECHO-QGP has an optical Glauber model as its default initial condition, which assumes independent linear trajectories of nucleons in nuclei that are distributed according to Woods-Saxon distribution [65,66]. Woods-Saxon distribution has a smooth plateau for the nucleus which decays softly towards the edges. Even though the Glauber model does not involve early stage dynamics and fluctuations of any kind, it is still a good approximation nonetheless.

IPGlasma [67,68] is a more realistic initial condition that includes the dynamics beginning from the moment of collision. It is based on the color glass condensate framework. The wave function of a nucleus or hadron at high energy could be explained with the effective theory of color glass condensate [69,70]. In the IPGlasma model, the color charges inside the nucleons are Gaussian sampled and are taken as the source for gluon fields, which are then evolved using clas-

sical Yang-Mills equations [67]. We have used the publicly available (see Ref. [71]) IPGlasma model that describes a boost-invariant $(2 + 1)$-D initial state. The energy density in
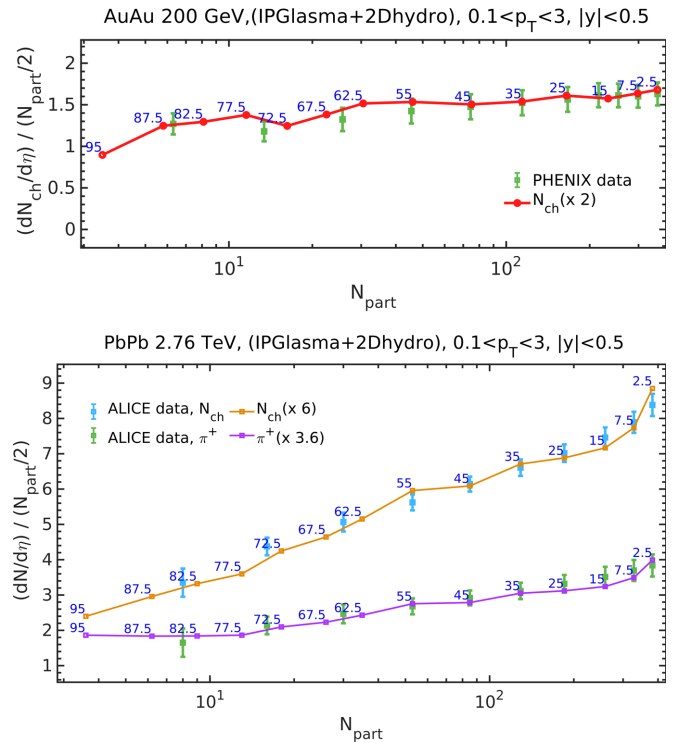

FIG. 3. Charged-particle multiplicity rapidity spectra generated (lines) for Au-Au 200 GeV (top panel) and Pb-Pb 2.76 TeV (bottom panel) as a function of the number of participants compared with corresponding PHENIX [40] and ALICE [42,43] experimental data (error bars). The generated data points are labeled with the midpoint of the centrality range in blue color.
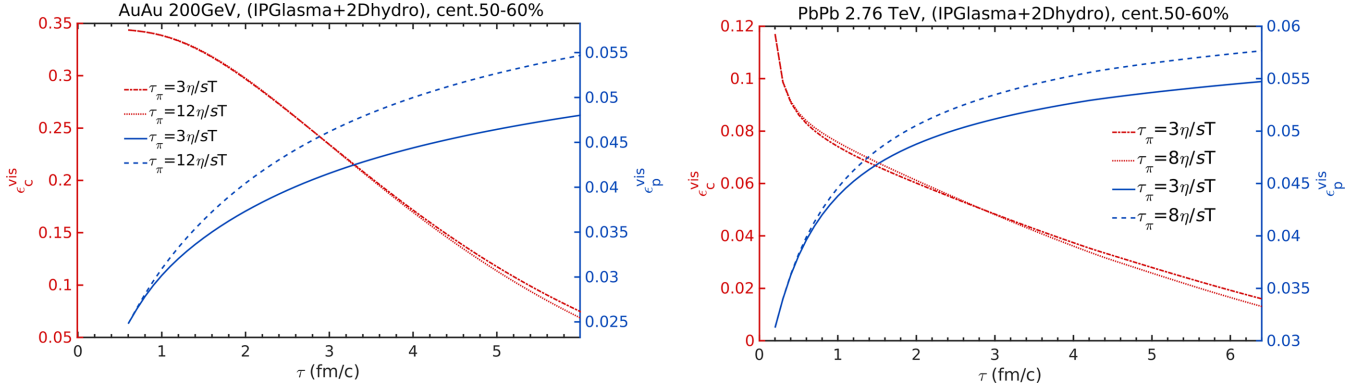
FIG. 4. Spatial eccentricity (red) and momentum space eccentricity (blue) for the viscous case for the Au-Au 200 GeV system (left) and the Pb-Pb 2.76 TeV system (right) for the two mentioned relaxation times at 50–60% centrality.

the transverse plane at $\tau_{\text{start}} = 0.2$ fm/c for Pb-Pb collision and $\tau_{\text{start}} = 0.6$ fm/c for Au-Au collision has been taken as an input for ECHO-QGP. Figure 1 shows the initial energy densities for 14 centralities as a function of transverse coordinates for Au-Au collision. We ran the (IPGlasma initial condition + ECHO-QGP hydrodynamics) framework for 14 centrality values, with more values near peripheral collisions.

The distribution of the nucleons in the nucleus and the distribution of the color charge inside nucleons are the key sources of initial state fluctuations in each collision event. Observables in collider experiments are averaged over a large number of collision events to account for this event-by-event fluctuation. For both Au-Au and Pb-Pb collision systems, we produce an initial state with 400 different sets of nucleon positions that are then combined into one. The total inelastic nucleon-nucleon cross section is set to 61.8 mb for the Pb-Pb system and 42 mb for the Au-Au system in both IPGlasma and hydrodynamics, taken from a Monte Carlo Glauber analysis [72]. The shear viscosity to entropy density ratio (η/s) is

taken as a constant, 0.1 ($\approx 1.25 \times \frac{1}{4\pi}$) [3], which is above the theoretical minimum Kovtun-Son-Starinets limit [73]. Bulk viscosity has not been included in this study. The pseudocritical temperature, at which the quarks to hadron phase transition occurs, has been calculated by various lattice QCD collaborations and is an input parameter. It is set to the recently calculated value of 156 MeV [74]. Chemical freeze-out is the point at which the inelastic scatterings cease to exist between produced hadrons. This point is decided by the temperature, which in the present model is fixed at 150 MeV [75].

B. Fixing centrality parameters

Figure 2 shows the p_T spectra of pions (π^+) produced for the two mentioned collision systems along with corresponding experimentally measured p_T spectra. The generated spectra adequately comply with experimental values only in the low-p_T regime, where the hydrodynamic mode operates. The energy density profile plotted as a function of the transverse
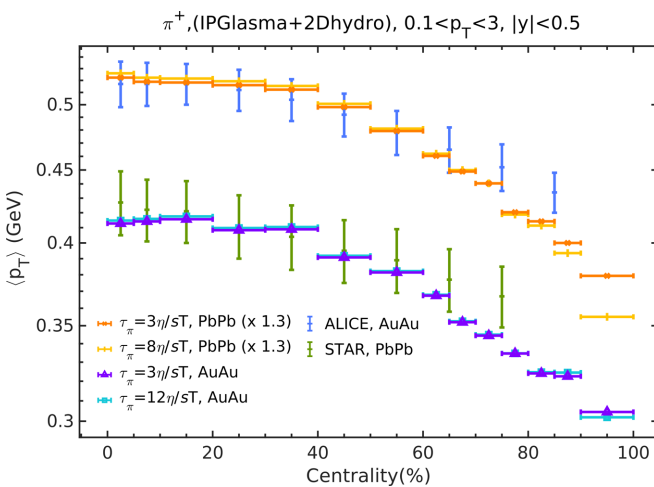

FIG. 5. Pion mean p_T as a function of centrality for Au-Au at 200 GeV and Pb-Pb at 2.76 TeV. The corresponding experimental data for PbPb from ALICE [42] and for AuAu from STAR [53] have systematic error bars.
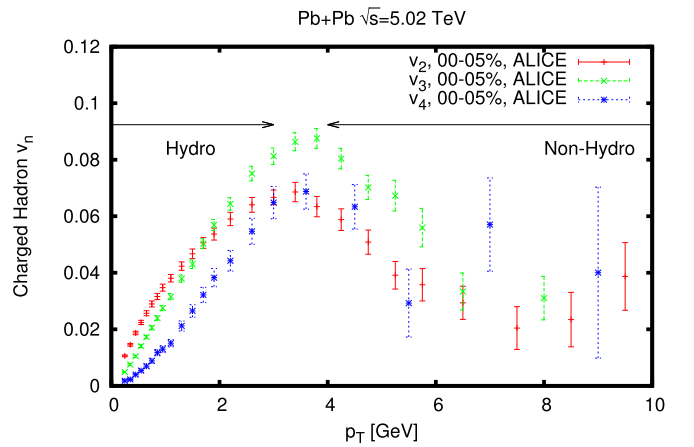

FIG. 6. Experimental values of flow coefficients as a function of transverse momentum. The plot is taken from Ref. [23]. Phenomenological studies that make use of viscous hydrodynamics have been able to explain flow experimental data only in the low-p_T range. Beyond $p_T \approx 4$ GeV, the presence of nonhydrodynamic mode has been suggested.
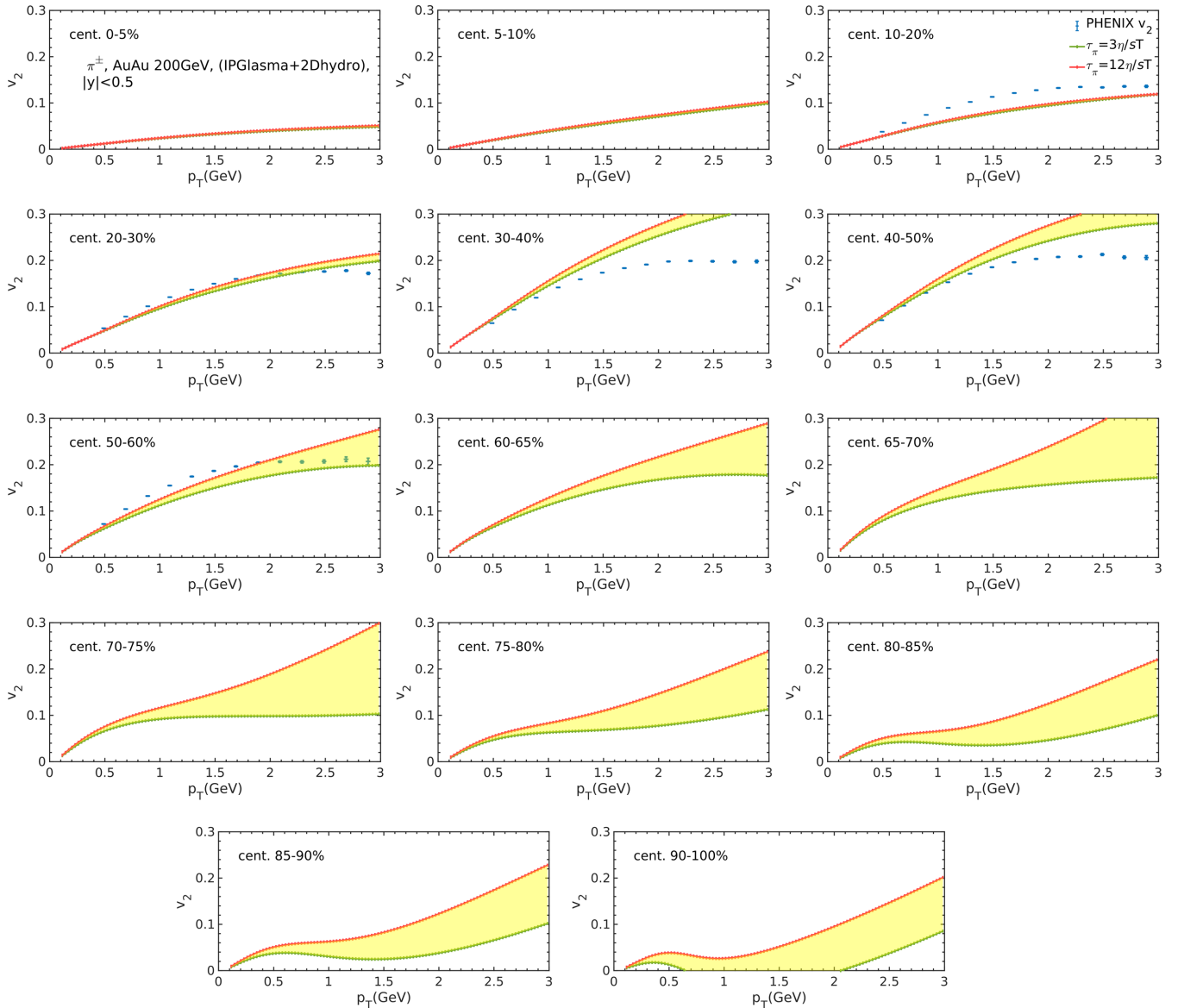
FIG. 7. Pion (π^+) elliptic flow coefficient (v_2) as a function of transverse momentum (p_T) for 14 centrality classes for the Au-Au 200 GeV system obtained with the IPGlasma + 2Dhydro setup along with experimentally measured elliptic flow (blue) from the PHENIX experiment [54] for the relaxation/nonhydrodynamic mode decay times $\tau_\pi = 3\eta/sT$ (green) and $\tau_\pi = 12\eta/sT$ (red). The shaded area (yellow) highlights the difference in flow due to variation in relaxation time.

coordinate from IPGlasma had to be scaled before being used in hydrodynamics. Figure 1 shows this scaled energy density distribution. This fixed the energy density scaling parameter such that the produced p_T spectra and the maxima of rapidity spectra (dN/dy) at each centrality match with the corresponding experimental measured data for both collision systems.

Figure 3 shows rapidity spectra normalized to $N_{part}/2$ as a function of N_{part}. In addition to the energy density scaling, the rapidity spectra had to be scaled to match with experimental results as shown in Fig. 3. For the Au-Au system, charged-particle normalized rapidity spectra were scaled up by a factor of 2, whereas for the Pb-Pb system this scaling was 6 and the corresponding scaling used for pions was 3.6. We chose a centrality range spaced by 5% in peripheral collisions except for the last centrality class, 90–100%. The impact parameter

and N_{part} values for all of these centrality ranges are taken from a Monte Carlo Glauber analysis [72]. The reason for taking more values towards the peripheral side was to capture fine variations of flow for decreasing dN/dy, as can be seen in Fig. 10 in Sec. III. However, there was no experimental reference to set parameters for these in-between centrality values for p_T spectra and the dN/dy vs N_{part} plot. Hence, we selected two values around each experimental centrality point starting from 60% as can be seen in the dN/dy vs N_{part} plot (Fig. 3). There was no experimental point at 90–100% so we settled with just one extrapolated value that follows the trend of the data. The blue labels on data points in Fig. 3 are the midcentrality values of those data points. For calculating observables for charged particles, we have added the corresponding values for the pions ($\pi^+ + \pi^-$), kaons ($K^+ + K^-$),
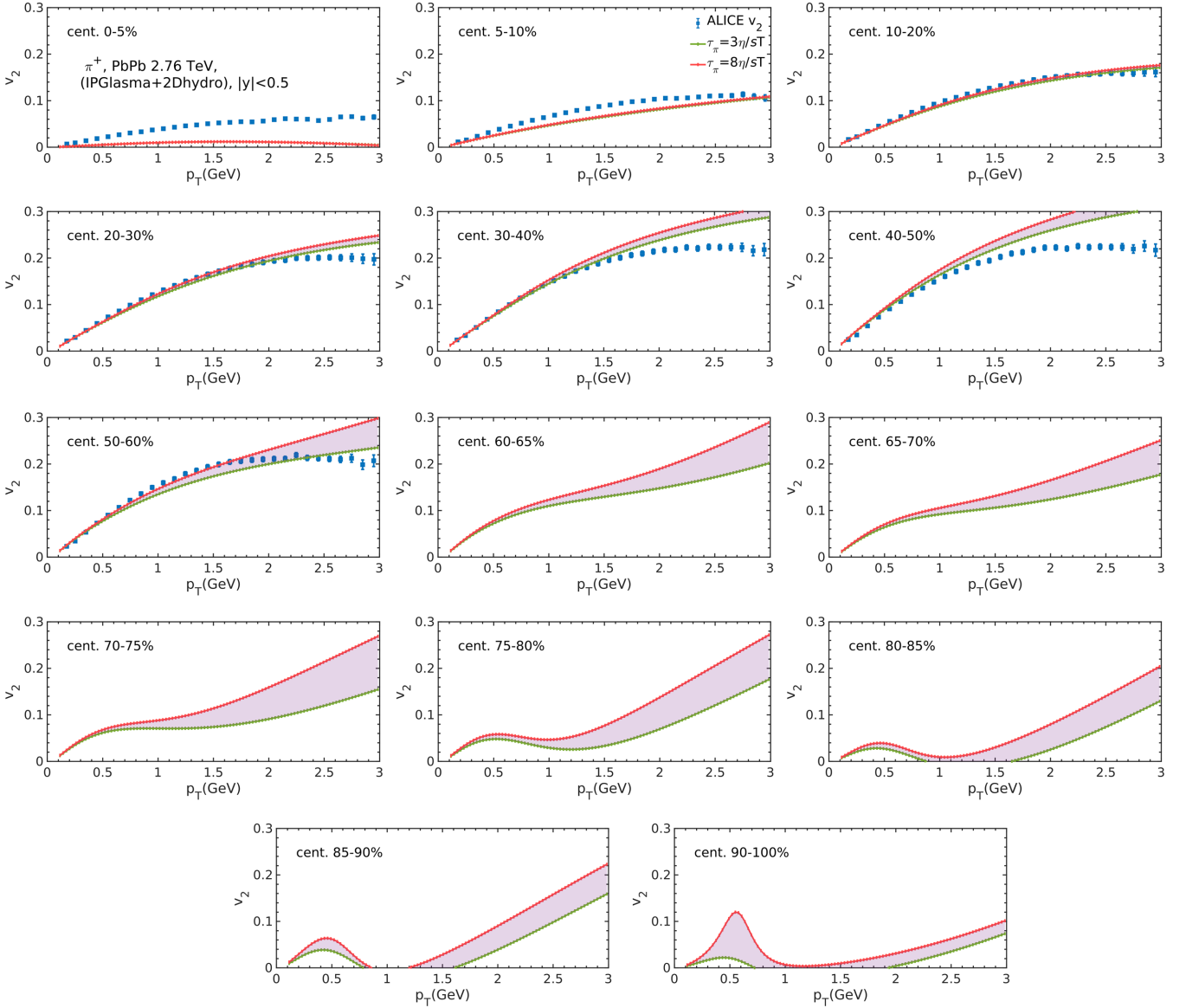
FIG. 8. Pion (π^+) elliptic flow coefficient as a function of transverse momentum (p_T) for 14 centrality classes for the Pb-Pb 2.76 TeV collision system obtained with IPGlasma + 2Dhydro setup along with elliptic flow measured at the ALICE experiment [55] (blue) for relaxation times $\tau_\pi = 3\eta/sT$ (green) and $\tau_\pi = 8\eta/sT$ (red). The shaded area (violet) highlights the difference in flow due to variation in relaxation time. See text for explanation.

and protons ($p^+ + p^-$) because these are abundantly produced species in high-energy collisions. Momentum space eccentricity, which is the precursor of elliptic flow, can be calculated in terms of $T^{\mu\nu}$ components as

$$e_p \equiv \frac{\int d^2x_\perp (T^{xx} - T^{yy})}{\int d^2x_\perp (T^{xx} + T^{yy})}. \qquad (13)$$

ECHO-QGP calculates this quantity for the ideal hydrodynamic case as:

$$e_p \equiv \frac{\int d^2x_\perp (\epsilon + P)(u^x u^x - u^y u^y)}{\int d^2x_\perp [(\epsilon + P)(u^x u^x + u^y u^y) + 2P]}. \qquad (14)$$

To generate momentum eccentricity for the viscous case, we have modified the above expression by adding a viscous component term, $\pi^{xx} + \pi^{yy}$, to the integrand in both the numerator and the denominator.

Figure 4 shows spatial eccentricity (ϵ_c) and momentum space eccentricity (ϵ_p) for Au-Au and Pb-Pb collisions, generated at 50–60% centrality for the two mentioned shear relaxation times. Momentum anisotropy quantified by momentum eccentricity increases at the expense of spatial anisotropy quantified by spatial eccentricities along the evolution [16]. The variation in the nonhydrodynamic mode decay time seems to have negligible effect on spatial eccentricity. The distinguishing feature between the two systems is that the early time ϵ_c for Pb-Pb collisions decreases more rapidly than

that for Au-Au collisions. Below the pseudocritical temperature, the hadronic picture should emerge. Particles of various species are assigned momentum according to the Cooper-Frye scheme [76]. The resulting momentum spectrum is then used to calculate the elliptic flow, $v_2 = \langle \cos[2(\phi - \Psi_{RP})] \rangle$, where Ψ_{RP} is the reaction plane angle which acts as a reference plane and ϕ is the transverse plane angle for a given particle with respect to the reaction plane.

Figure 5 shows the average transverse momentum evolution as a function of centrality. Results for the two values of shear relaxation time have been plotted and compared with experimental values for pions. We notice that the model shows agreement with experimental values for most of the centrality classes apart from the peripheral ones. The values for Pb-Pb collisions had to be scaled up by a factor of 1.3. This could be due to underproduction of hadrons in the hydrodynamics, because the multiplicity has been used as the weight factor for calculating the mean p_T.

III. FLOW RESULTS AND DISCUSSION

Romatschke [23] has put forth a quantitative test for applicability of hydrodynamics by checking the sensitivity of certain observables (like elliptic flow) to the nonhydrodynamic mode. The idea is that hydrodynamics can be used to describe a system if the nonhydrodynamic mode is subdominant and there exists a local rest frame. With QCD as the microscopic theory, the approximate transverse momentum range of the hydrodynamic mode is 3 to 7 GeV. Figure 6 illustrates this p_T range where hydro and nonhydro modes operate.

This is what we have tried checking for the Au-Au 200 GeV system in Fig. 7 and for the Pb-Pb 2.76 TeV system in Fig. 8. Peripheral collisions are the system of interest, but experimentally measured anisotropic flow results are only available up to the 50–60% centrality class. We hence presented the results for the complete centrality range. In Fig. 7, for 0–5%, 5–10%, and 10–20% centralities, we see no separation between elliptic flow curves for nonhydrodynamic mode decay times, $\tau_\pi = 3\eta/sT$ and $12\eta/sT$. From the 20–30% centrality class onwards we notice the separation between these two flow curves to be increasing. Experimental data have been plotted just for reference that show our results are quite close to experimentally measured flow results. The important point to notice is that along the increasing centrality, the point at which the two flow curves separate shifts towards lower p_T values, which means that with increasing centrality and decreasing system size, the hydrodynamic mode is shrinking and the nonhydrodynamic mode is getting dominant. Hence, in a way, we are witnessing the limit of applicability of low-order hydrodynamics for decreasing system size at constant collisional energy (here, 200 GeV).

Figure 8 shows the p_T dependence of the pion (π^+) elliptic flow with the complete centrality range for $\tau_\pi = 3\eta/sT$ and $8\eta/sT$. We notice all the structures mentioned above for the Au-Au 200 GeV system. We notice a better match between the produced elliptic flow and experimental data for 10–20% onwards. We chose pions for this analysis because they are the lightest of particle species produced and hence adequately
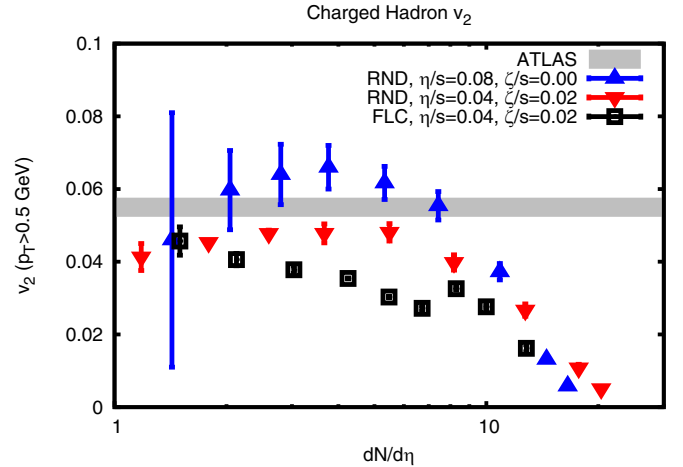

FIG. 9. p_T-integrated elliptic flow in proton-proton collision at 7 TeV, produced using the SONIC model, as a function of multiplicity pseudorapidity spectra for the mentioned values of η/s and ζ/s. For $\eta/s = 0.08$ and $\zeta/s = 0$ (blue), the elliptic flow has error bars due to variation in shear relaxation or nonhydro mode decay time, which increase in size for decreasing $dN/d\eta$. The plot is taken from Ref. [23].

represent the bulk medium. One additional point to notice is that, for 10–20% centrality in Au-Au collisions and classes 0–5% and 5–10% in the Pb-Pb collision system, our model fails to reproduce the measured elliptic flow data.

Figure 9 depicts the criteria suggested by Romatschke [23] to check the applicability of hydrodynamics. This figure shows charged-particle elliptic flow as a function of the multiplicity pseudorapidity density for proton-proton collisions. The error bars depict the abrupt change in flow due to variation in the nonhydrodynamic mode decay time. This abrupt change in elliptic flow is indicative of the breakdown of hydrodynamics, and it is seemingly happening at roughly $dN/d\eta < 2$ in Fig. 9. We tried checking this feature in our IPGlasma + 2Dhydro analysis as shown in Figs. 11 and 10.

Figure 10 presents the un-normalized p_T-integrated elliptic flow as a function of the multiplicity rapidity density (dN/dy). The data points from our analysis are labeled by the centrality class in order to track the point at which the flow changes abruptly between the relaxation time curves. This is why we selected more centrality points on the peripheral collision side. We notice a steady increase in separation between the two flow curves for both the Au-Au system and the Pb-Pb system, which is in reasonably close agreement with Romatschke's work [23].

We also notice that the two relaxation time flow curves of the same centrality do not have the same multiplicity rapidity density value (the x coordinate). This would mean that, for an increase in the relaxation time, the flow shifts to a lower multiplicity value. We also notice that the flow for $\tau_\pi = 3\eta/sT$ for both the Au-Au system and the Pb-Pb system acquires negative values, which is also apparent from the elliptic flow for the 90–100% centrality class in Figs. 8 and 7.

Figure 11 shows normalized p_T-integrated elliptic flow as a function of the charged-particle multiplicity rapidity
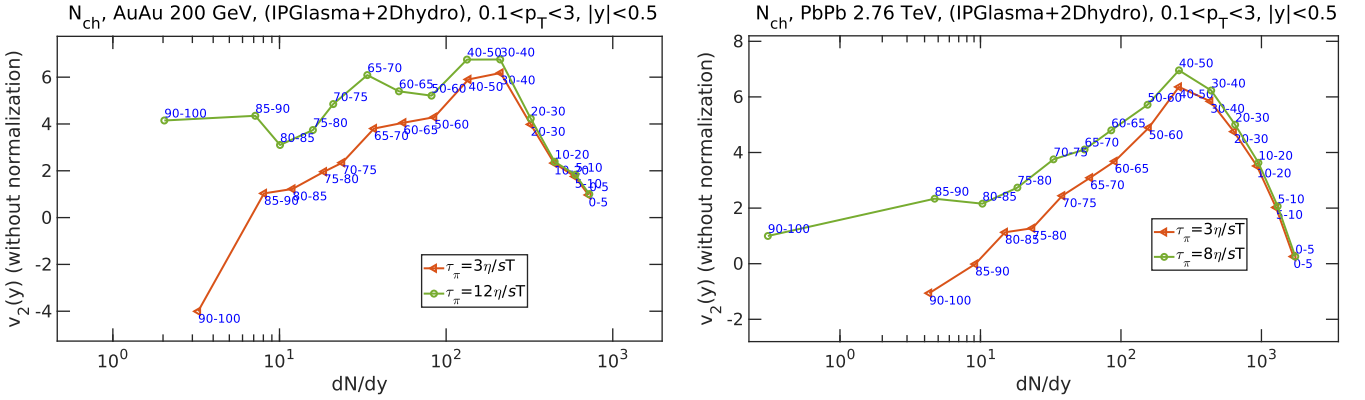
FIG. 10. Un-normalized p_T-integrated elliptic flow of charged particles as a function of N_{ch} rapidity density for AuAu 200 GeV (left) and Pb-Pb 2.76 TeV (right) systems plotted for the two mentioned relaxation times. Data points are labeled by the centrality values. The separation between the two curves along the complete centrality range is better seen for the un-normalized elliptic flow than for the normalized one in Fig. 11.

density (dN/dy) for peripheral collisions. We clearly notice the sudden increase in separation of flow curves for the two mentioned relaxation times for both the collision systems, but we do not have a centrality resolution good enough to decide the onset of hydrodynamization. An approximate limit we can deduce from Fig. 11 is $dN/dy \approx 10$, which is quite larger than the prediction of $dN/d\eta < 2$ [23,34]. However, if the hadron resonance gas to deconfined quarks transition in the high-temperature regime is a crossover, we expect to find a region where analysis would be indecisive like what Kurkela *et al.* obtained [32,33]. The problem lies in the absence of experimental reference data to set the scaling parameter of IPGlasma for such high-centrality classes.

IV. CONCLUSION AND OUTLOOK

In this study we analyze the nonhydrodynamic mode in an attempt to find the onset of hydrodynamization in peripheral collision systems of Au-Au and Pb-Pb at 200 GeV and 2.76 TeV center of mass per energy nucleon, respectively. We use the energy density profile from the *color glass condensate*-based IPGlasma model as the initial condition in 2D ECHO-QGP, which is a second-order viscous hydrodynamic

code based on the MIS theory. p_T spectra and multiplicity rapidity density [$dN/dy/(N_{part}/2)$] as a function of N_{part} are used to constrain the centrality scaling parameter of IP-Glasma. Mean p_T as a function of centrality and evolution of spatial and momentum eccentricity has also been generated for both the systems. The shear viscosity to entropy density ratio is set as $\eta/s = 0.1$ and bulk viscosity has not been considered in this work. We study the variation in the strength of the nonhydrodynamic mode through the shear relaxation time, whose value is set to $(3–12)\eta/sT$ for the Au-Au system and $(3–8)\eta/sT$ for the Pb-Pb system. Elliptic flow generated as a function of p_T is compared with the experimentally measured elliptic flow for the above respective values of relaxation time, for all of the 14 centrality classes. Normalized and un-normalized p_T-integrated elliptic flow has been studied as a function of the multiplicity rapidity density in peripheral collisions especially. We found the following.

(i) From the p_T dependence of elliptic flow across centralities for Au-Au in Fig. 7 and for Pb-Pb in Fig. 8, we found that the shear relaxation time does control the nonhydrodynamic mode of the system as predicted by Romatschke [23]. This inference was
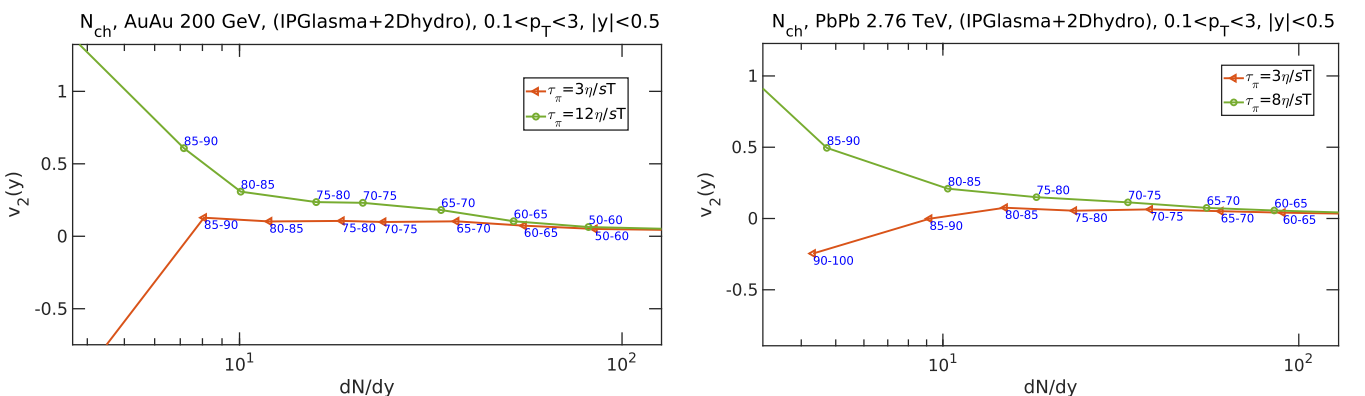

FIG. 11. p_T-integrated elliptic flow of charged particles as a function of N_{ch} rapidity density for Au-Au 200 GeV (left) and Pb-Pb 2.76 TeV (right) plotted for the two mentioned relaxation times. Data points are labeled by the centrality values. See text for explanation.

guided by the observation that the point after which the flows for the two relaxation times separate sharply from each other, shifts to lower p_T values for increasing centrality classes (or decreasing system size at a constant energy of collision).

(ii) We later attempted testing the onset of hydrodynamization from charged-particle multiplicity rapidity density dependence of p_T-integrated elliptic flow. We did notice an abrupt increase in flow for decreasing system size or number of participants, indicating increased dominance of the nonhydrodynamic mode and simultaneous breakdown of hydrodynamic description. However, we could not resolve the dN/dy below the value of 10 enough to quantitatively decide the onset point.

(iii) We found a good agreement between the generated p_T dependence of elliptic flow results and the measured flow data from the PHENIX and ALICE Collaborations for Au-Au and Pb-Pb systems, respectively, except near most centrality of the 10–20% class for Au-Au collisions and of the 0–5% and 5–10% classes for Pb-Pb collisions.

There is significant scope for improving this framework further by including an afterburner stage that will incorporate hadron resonance decays and scattering which could affect the generated flow [77]. It will be interesting to compare the lowest fluid size from other methods in future work. The initial state involvement could also be improved by using more components of $T^{\mu\nu}$ in hydrodynamics [78,79]. One can also switch to a 3D IPGlasma initial condition [80]. Bulk viscosity has been kept zero in this study, but it does play a significant role in evolution [81]. The relaxation times for bulk viscosity could be independently analyzed. It will be interesting to see if the elliptic flows of different particle species diverge for decreasing rapidity spectra at different points. If they do so, it would support the idea of a multiple-fluid scenario in heavy-ion collisions. This study could be extended to small and lower-energy systems where the net-baryon potential is nonzero, for which particle current conservation should be included [82]. In a recent study, Plumberg *et al.* [83] have conducted a causality analysis of each fluid cell of hydrodynamics for its complete evolution. They found causality violation of nonhyperbolic ($v^2 < 0$) and superluminal ($v^2 > c^2$) type in the early time evolution of viscous hydrodynamics. This violation is significantly reduced if a pre-equilibrium stage like KøMPøST [84] is used. It will be interesting to see the repercussions of such a study on the onset of hydrodynamization.

ACKNOWLEDGMENTS

[1] E. V. Shuryak, Theory of hadron plasma, Zh. Eksp. Teor. Fiz. **74**, 408 (1978) [Sov. Phys. JETP **47**, 212 (1978)].

[2] E. V. Shuryak, Quantum chromodynamics and the theory of superdense matter, Phys. Rep. **61**, 71 (1980).

[3] W. Busza, K. Rajagopal, and W. Van Der Schee, Heavy ion collisions: the big picture and the big questions, Annu. Rev. Nucl. Part. Sci. **68**, 339 (2018).

[4] F. Karsch, E. Laermann, and A. Peikert, Quark mass and flavour dependence of the QCD phase transition, Nucl. Phys. B **605**, 579 (2001).

[5] J. Berges, M. P. Heller, A. Mazeliauskas, and R. Venugopalan, QCD thermalization: *Ab initio* approaches and interdisciplinary connections, Rev. Mod. Phys. **93**, 035003 (2021).

[6] J. Casalderrey-Solana, M. P. Heller, D. Mateos, and W. van der Schee, Longitudinal Coherence in a Holographic Model of Asymmetric Collisions, Phys. Rev. Lett. **112**, 221602 (2014).

[7] J. Letessier and J. Rafelski, Observing quark-gluon plasma with strange hadrons, Int. J. Mod. Phys. E **09**, 107 (2000).

[8] K. Ackermann, N. Adams, C. Adler, Z. Ahammed, S. Ahmad, C. Allgower, J. Amsbaugh, M. Anderson, E. Anderssen, H. Arnesen *et al.*, Elliptic Flow in Au+Au Collisions at $\sqrt{s_{NN}} = $ 130 GeV, Phys. Rev. Lett. **86**, 402 (2001).

[9] K. Adcox *et al.* (PHENIX Collaboration), Suppression of Hadrons with Large Transverse Momentum in Central Au + Au Collisions at $\sqrt{s_{NN}} = $ 130 GeV, Phys. Rev. Lett. **88**, 022301 (2001).

[10] C. Adler *et al.* (STAR Collaboration), Disappearance of Back-to-Back High-p_T Hadron Correlations in Central Au + Au Collisions at $\sqrt{s_{NN}} = $ 200 GeV, Phys. Rev. Lett. **90**, 082302 (2003).

[11] G. Odyniec, The RHIC beam energy scan program in STAR and what's next.., J. Phys.: Conf. Ser. **455**, 012037 (2013).

[12] J. E. Bernhard, J. S. Moreland, and S. A. Bass, Bayesian estimation of the specific shear and bulk viscosity of quark–gluon plasma, Nat. Phys. **15**, 1113 (2019).

[13] T.-Y. Wu and P. W. Hwang, *Relativistic Quantum Mechanics and Quantum Fields* (World Scientific, Singapore, 1991).

[14] C. Ratti, Lattice QCD and heavy ion collisions: a review of recent progress, Rep. Prog. Phys. **81**, 084301 (2018).

[15] A. Bazavov, T. Bhattacharya, C. DeTar, H.-T. Ding, S. Gottlieb, R. Gupta, P. Hegde, U. Heller, F. Karsch, E. Laermann, L. Levkova, S. Mukherjee, P. Petreczky, C. Schmidt, C. Schroeder, R. A. Soltz, W. Soeldner, R. Sugar, M. Wagner, and P. Vranas, Equation of state in (2+1)-flavor QCD, Phys. Rev. D **90**, 094503 (2014).

[16] M. Luzum and P. Romatschke, Conformal relativistic viscous hydrodynamics: Applications to RHIC results at $\sqrt{s_{NN}} = $ 200 GeV, Phys. Rev. C **78**, 034915 (2008).

[17] P. Romatschke, New developments in relativistic viscous hydrodynamics, Int. J. Mod. Phys. E **19**, 1 (2010).

[18] P. Kovtun, Lectures on hydrodynamic fluctuations in relativistic theories, J. Phys. A: Math. Theor. **45**, 473001 (2012).

[19] S. Jeon and U. Heinz, Introduction to hydrodynamics, Int. J. Mod. Phys. E **24**, 1530010 (2015).

[20] A. Jaiswal and V. Roy, Relativistic hydrodynamics in heavy-ion collisions: general aspects and recent developments, Adv. High Energy Phys. **2016**, 9623034 (2016).

[21] W. Florkowski, M. P. Heller, and M. Spaliński, New theories of relativistic hydrodynamics in the LHC era, Rep. Prog. Phys. **81**, 046001 (2018).

[22] J.-P. Blaizot and L. Yan, Emergence of hydrodynamical behavior in expanding ultra-relativistic plasmas, Ann. Phys. **412**, 167993 (2020).

[23] P. Romatschke, Do nuclear collisions create a locally equilibrated quark–gluon plasma? Eur. Phys. J. C **77**, 21 (2017).

[24] M. P. Heller, R. A. Janik, and P. Witaszczyk, Hydrodynamic Gradient Expansion in Gauge Theory Plasmas, Phys. Rev. Lett. **110**, 211602 (2013).

[25] M. P. Heller and M. Spaliński, Hydrodynamics Beyond the Gradient Expansion: Resurgence and Resummation, Phys. Rev. Lett. **115**, 072501 (2015).

[26] P. Romatschke, Relativistic hydrodynamic attractors with broken symmetries: non-conformal and non-homogeneous, J. High Energy Phys. 12 (2017) 079.

[27] A. Kurkela, W. van der Schee, U. A. Wiedemann, and B. Wu, Early- and Late-Time Behavior of Attractors in Heavy-Ion Collisions, Phys. Rev. Lett. **124**, 102301 (2020).

[28] P. Castorina, A. Iorio, D. Lanteri, H. Satz, and M. Spousta, Universality in hadronic and nuclear collisions at high energy, Phys. Rev. C **101**, 054902 (2020).

[29] B. Schenke, C. Shen, and P. Tribedy, Running the gamut of high energy nuclear collisions, Phys. Rev. C **102**, 044905 (2020).

[30] M. Habich, G. A. Miller, P. Romatschke, and W. Xiang, Testing hydrodynamic descriptions of p+p collisions at $\sqrt{s} = 7$ TeV, Eur. Phys. J. C **76**, 408 (2016).

[31] J. L. Nagle and W. A. Zajc, Small system collectivity in relativistic hadronic and nuclear collisions, Annu. Rev. Nucl. Part. Sci. **68**, 211 (2018).

[32] A. Kurkela, U. A. Wiedemann, and B. Wu, Flow in AA and pA as an interplay of fluid-like and non-fluid like excitations, Eur. Phys. J. C **79**, 965 (2019).

[33] A. Kurkela, U. A. Wiedemann, and B. Wu, Opacity dependence of elliptic flow in kinetic theory, Eur. Phys. J. C **79**, 759 (2019).

[34] U. Heinz and J. S. Moreland, Hydrodynamic flow in small systems or: "how the heck is it possible that a system emitting only a dozen particles can be described by fluid dynamics"? J. Phys.: Conf. Ser. **1271**, 012018 (2019).

[35] H. Song and U. Heinz, Multiplicity scaling in ideal and viscous hydrodynamics, Phys. Rev. C **78**, 024902 (2008).

[36] H. Song and U. Heinz, Causal viscous hydrodynamics in $2 + 1$ dimensions for relativistic heavy-ion collisions, Phys. Rev. C **77**, 064901 (2008).

[37] H. Song and U. Heinz, Suppression of elliptic flow in a minimally viscous quark–gluon plasma, Phys. Lett. B **658**, 279 (2008).

[38] H. Niemi, G. S. Denicol, P. Huovinen, E. Molnár, and D. H. Rischke, Influence of a temperature-dependent shear viscosity on the azimuthal asymmetries of transverse momentum spectra in ultrarelativistic heavy-ion collisions, Phys. Rev. C **86**, 014909 (2012).

[39] G. Nijs, W. van der Schee, U. Gürsoy, and R. Snellings, Bayesian analysis of heavy ion collisions with the heavy ion computational framework TRAJECTUM, Phys. Rev. C **103**, 054909 (2021).

[40] S. S. Adler *et al.* (PHENIX Collaboration), Identified charged particle spectra and yields in Au + Au collisions at $\sqrt{s_{NN}} = 200$ GeV, Phys. Rev. C **69**, 034909 (2004).

[41] J. Adam, Adagmar, M. M. Aggarwal, G. A. Rinella, M. Agnello, N. Agrawal, Z. Ahammed, S. U. Ahn, I. Aimo, S. Aiola *et al.*, Centrality dependence of the nuclear modification factor of charged pions, kaons, and protons in Pb-Pb collisions at $\sqrt{s_{NN}} = 2.76$ TeV, Phys. Rev. C **93**, 034913 (2016).

[42] B. Abelev *et al.* (ALICE Collaboration), Centrality dependence of π, K, and p production in Pb-Pb collisions at $\sqrt{s_{NN}} = 2.76$ TeV, Phys. Rev. C **88**, 044910 (2013).

[43] K. Aamondt *et al.* (ALICE Collaboration), Centrality Dependence of the Charged-Particle Multiplicity Density at Midrapidity in Pb-Pb Collisions at $\sqrt{s_{NN}} = 2.76$ TeV, Phys. Rev. Lett. **106**, 032301 (2011).

[44] C. Eckart, The thermodynamics of irreversible processes. III. Relativistic theory of the simple fluid, Phys. Rev. **58**, 919 (1940).

[45] I. Möller, Zum paradoxon der wärmeleitungstheorie, Z. Phys. **198**, 329 (1967).

[46] W. Israel, Nonstationary irreversible thermodynamics: a causal relativistic theory, Ann. Phys. **100**, 310 (1976).

[47] W. Israel and J. M. Stewart, Transient relativistic thermodynamics and kinetic theory, Ann. Phys. **118**, 341 (1979).

[48] G. S. Denicol, T. Koide, and D. H. Rischke, Dissipative Relativistic Fluid Dynamics: A New Way to Derive the Equations of Motion from Kinetic Theory, Phys. Rev. Lett. **105**, 162501 (2010).

[49] R. Baier, P. Romatschke, D. T. Son, A. O. Starinets, and M. A. Stephanov, Relativistic viscous hydrodynamics, conformal invariance, and holography, J. High Energy Phys. 04 (2008) 100.

[50] A. Jaiswal, Relativistic third-order dissipative fluid dynamics from kinetic theory, Phys. Rev. C **88**, 021903(R) (2013).

[51] S. M. Diles, L. A. Mamani, A. S. Miranda, and V. T. Zanchin, Third-order relativistic hydrodynamics: dispersion relations and transport coefficients of a dual plasma, J. High Energy Phys. 05 (2020) 019.

[52] http://theory.fi.infn.it/echoqgp/index.php.

[53] B. I. Abelev *et al.* (STAR Collaboration), Systematic measurements of identified particle spectra in pp, $d + $Au, and Au + Au collisions at the STAR detector, Phys. Rev. C **79**, 034909 (2009).

[54] S. Afanasiev *et al.* (PHENIX Collaboration), Systematic studies of elliptic flow measurements in Au + Au collisions at $\sqrt{s_{NN}} = 200$ GeV, Phys. Rev. C **80**, 024909 (2009).

[55] B. Chang, D. J. Kim, J. Kral, E. Pohjoisaho, S. Rak, S. Räsänen, M. Slupecki, W. Trzaska, M. Vargyas, J. Viinikainen *et al.*, Elliptic flow of identified hadrons in Pb-Pb collisions at $\sqrt{s_{NN}} = 2.76$ TeV, J. High Energy Phys. 06 (2015) 190.

[56] L. Del Zanna, V. Chandra, G. Inghirami, V. Rolando, A. Beraudo, A. De Pace, G. Pagliara, A. Drago, and F. Becattini, Relativistic viscous hydrodynamics for heavy-ion collisions with ECHO-QGP, Eur. Phys. J. C **73**, 2524 (2013).

[57] V. Rolando, G. Inghirami, A. Beraudo, L. Del Zanna, F. Becattini, V. Chandra, A. De Pace, and M. Nardi, Heavy ion collision evolution modeling with ECHO-QGP, Nucl. Phys. A **931**, 970 (2014).

[58] N. Hatwar, C. R. Singh, S. Ganesh, and M. Mishra, Bottomonium suppression in PbPb collisions at energies available at the CERN Large Hadron Collider, Phys. Rev. C **104**, 034905 (2021).

[59] S. Borsányi, G. Endrődi, Z. Fodor, A. Jakovac, S. D. Katz, S. Krieg, C. Ratti, and K. K. Szabó, The QCD equation of state with dynamical quarks, J. High Energy Phys. 11 (2010) 077.

[60] S. Chatterjee, R. M. Godbole, and S. Gupta, Stabilizing hadron resonance gas models, Phys. Rev. C **81**, 044907 (2010).

[61] R. Baier, P. Romatschke, and U. A. Wiedemann, Dissipative hydrodynamics and heavy-ion collisions, Phys. Rev. C **73**, 064903 (2006).

[62] M. A. York and G. D. Moore, Second order hydrodynamic coefficients from kinetic theory, Phys. Rev. D **79**, 054011 (2009).

[63] M. P. Heller and R. A. Janik, Viscous hydrodynamics relaxation time from AdS/CFT correspondence, Phys. Rev. D **76**, 025027 (2007).

[64] S. Bhattacharyya, R. Loganayagam, I. Mandal, S. Minwalla, and A. Sharma, Conformal nonlinear fluid dynamics from gravity in arbitrary dimensions, J. High Energy Phys. 12 (2008) 116.

[65] P. F. Kolb, U. Heinz, P. Huovinen, K. J. Eskola, and K. Tuominen, Centrality dependence of multiplicity, transverse energy, and elliptic flow from hydrodynamics, Nucl. Phys. A **696**, 197 (2001).

[66] M. L. Miller, K. Reygers, S. J. Sanders, and P. Steinberg, Glauber modeling in high-energy nuclear collisions, Annu. Rev. Nucl. Part. Sci. **57**, 205 (2007).

[67] B. Schenke, P. Tribedy, and R. Venugopalan, Fluctuating Glasma Initial Conditions and Flow in Heavy Ion Collisions, Phys. Rev. Lett. **108**, 252301 (2012).

[68] B. Schenke, P. Tribedy, and R. Venugopalan, Event-by-event gluon multiplicity, energy density, and eccentricities in ultrarelativistic heavy-ion collisions, Phys. Rev. C **86**, 034908 (2012).

[69] L. McLerran and R. Venugopalan, Computing quark and gluon distribution functions for very large nuclei, Phys. Rev. D **49**, 2233 (1994).

[70] F. Gelis, E. Iancu, J. Jalilian-Marian, and R. Venugopalan, The color glass condensate, Annu. Rev. Nucl. Part. Sci. **60**, 463 (2010).

[71] https://github.com/schenke/ipglasma.

[72] C. Loizides, J. Kamin, and D. d'Enterria, Improved Monte Carlo Glauber predictions at present and future nuclear colliders, Phys. Rev. C **97**, 054910 (2018).

[73] P. K. Kovtun, D. T. Son, and A. O. Starinets, Viscosity in Strongly Interacting Quantum Field Theories from Black Hole Physics, Phys. Rev. Lett. **94**, 111601 (2005).

[74] H.-T. Ding, New developments in lattice QCD on equilibrium physics and phase diagram, Nucl. Phys. A **1005**, 121940 (2021).

[75] A. Mazeliauskas and V. Vislavicius, Temperature and fluid velocity on the freeze-out surface from π, K, and p spectra in pp, p-Pb, and Pb-Pb collisions, Phys. Rev. C **101**, 014910 (2020).

[76] F. Cooper and G. Frye, Single-particle distribution in the hydrodynamic and statistical thermodynamic models of multiparticle production, Phys. Rev. D **10**, 186 (1974).

[77] S. A. Bass, M. Belkacem, M. Bleicher, M. Brandstetter, L. Bravina, C. Ernst, L. Gerland, M. Hofmann, S. Hofmann, J. Konopka *et al.*, Microscopic models for ultrarelativistic heavy ion collisions, Prog. Part. Nucl. Phys. **41**, 255 (1998).

[78] C. Chattopadhyay, R. S. Bhalerao, J.-Y. Ollitrault, and S. Pal, Effects of initial-state dynamics on collective flow within a coupled transport and viscous hydrodynamic approach, Phys. Rev. C **97**, 034915 (2018).

[79] B. Schenke, C. Shen, and P. Tribedy, Hybrid color glass condensate and hydrodynamic description of the relativistic heavy ion collider small system scan, Phys. Lett. B **803**, 135322 (2020).

[80] B. Schenke and S. Schlichting, 3D glasma initial state for relativistic heavy ion collisions, Phys. Rev. C **94**, 044907 (2016).

[81] S. Ryu, J.-F. Paquet, C. Shen, G. S. Denicol, B. Schenke, S. Jeon, and C. Gale, Importance of the Bulk Viscosity of QCD in Ultrarelativistic Heavy-Ion Collisions, Phys. Rev. Lett. **115**, 132301 (2015).

[82] L. Du and U. Heinz, $(3 + 1)$-dimensional dissipative relativistic fluid dynamics at non-zero net baryon density, Comput. Phys. Commun. **251**, 107090 (2020).

[83] C. Plumberg, D. Almaalol, T. Dore, J. Noronha, and J. Noronha-Hostler, Causality violations in realistic simulations of heavy-ion collisions, Phys. Rev. C **105**, L061901 (2022).

[84] A. Kurkela, A. Mazeliauskas, J.-F. Paquet, S. Schlichting, and D. Teaney, Effective kinetic description of event-by-event pre-equilibrium dynamics in high-energy heavy-ion collisions, Phys. Rev. C **99**, 034910 (2019).